IEEE Access
Multidisciplinary | Rapid Review | Open Access Journal

Received January 4, 2019, accepted January 16, 2019, date of publication January 23, 2019, date of current version February 8, 2019.

Digital Object Identifier 10.1109/ACCESS.2019.2894345

Simulation of the Separating Crowd Behavior in a T-Shaped Channel Based on the Social Force Model

ZHILU YUAN, RENZHONG GUO, SHENGJUN TANG, BIAO HE, LEI BIAN, AND YOU LI

Shenzhen Key Laboratory of Spatial Information Smart Sensing and Services, School of Architecture and Urban Planning, Research Institute for Smart Cities, Shenzhen University, Shenzhen 518060, China

Corresponding author: Biao He (whu_hebiao@hotmail.com)

This work was supported in part by the NSFC under Grant 51278221, Grant 51378076, Grant 41701187, and Grant 20170101155JC (Jilin Science and Technology Development Program), in part by the National Natural Science Foundation of China under Grant 41801392, in part by the China Postdoctoral Science Foundation under Grant 2018M640821, Grant 2018M633133, and Grant 2018M643150, in part by the Open Fund of Key Laboratory of Urban Land Resources Monitoring and Simulation under Grant KF-2018-03-031, and in part by the Ministry of Land and Resources, Shenzhen, China.

ABSTRACT The separating behavior defines the division of a crowd from a single flow into two distributary flows due to the different pedestrians' destinations. Nevertheless, in the existing literature on pedestrian flow, there is a lack of simulation research on the separating crowd behavior in a T-shaped channel. By conducting a series of controlled experiments, we analyzed the moving trajectories and the spatial and temporal distribution characteristics of pedestrians in the separation process. Based on an analysis of the controlled experiments, we proposed an improved social force model that fully considers the characteristics of pedestrians' swapping locations, and refines the directions of pedestrians' expected speeds in three stages of the pedestrian separation process. During the simulation, we applied the improved model to explore the effects of the pedestrians' swapping locations on the macroscopic phenomena, microscopic individual behavior, and traffic efficiency within a T-shaped channel. The simulation results show that if pedestrians' swapping locations are concentrated in a certain area close to the entrance, the traffic efficiency in the T-shaped channel will be higher than that if the pedestrians' swapping locations are dispersed. Moreover, as the flow rate at the entrance increases, the swapping location becomes more concentrated closer to the entrance, the mean speed increases, and fewer conflicts occur between the pedestrians.

INDEX TERMS Crowd safety, pedestrian dynamics, swapping location, traffic optimization.

I. INTRODUCTION

With increases in the size and frequency of mass events, studies of crowd disasters and simulations of pedestrian flows have become important research areas [1]. Pedestrians exhibit complex movement behaviors during various maneuvers, including turning, crossing, merging and separating, and these complex movements directly affect the efficiency of building evacuations and the safety of pedestrians. As an effective means of analyzing the characteristics of pedestrian movement behaviors, crowd simulations can synthetically reproduce the individual movement behaviors of pedestrians, the interactions among pedestrians and the influences of the walking environment on pedestrians. Accordingly, research involving simulations of pedestrian flow has tremendous significance for evacuation analysis, passenger transport hub design and traffic optimization [2].

Researchers have conducted targeted research on the behavioral characteristics of pedestrians according to different real dynamic scenarios; the corresponding studies can be divided into the following representative research categories. One category involves counter flow within a bidirectional channel [3]–[7]; this kind of research focuses on the behaviors and decision-making processes associated with counter flow during the crossing process and the influencing factors of the lane formation phenomenon. For this purpose, researchers have modeled a variety of behaviors, including those associated with walking sideways, the following behavior, and the right-preference behavior of counter flow. Another category involves pedestrian flow in a narrow bottleneck [8]–[11]; this research focuses on organizing the movements between two groups of pedestrians so that they can efficiently pass through a bottleneck in opposite

directions [12]. Accordingly, researchers have modeled the spatial and temporal separation rules of pedestrian flow in a narrow bottleneck and analyzed the influencing factors on oscillatory flow and the lane formation phenomenon in a narrow bottleneck. The evacuation flow in a room constitutes another research topic [13]–[15] that focuses on the evacuation flow in a room under emergency conditions. For this category, researchers have considered the influences of panic, smoke, fire evacuation and emergency signs on the movements of pedestrians with the ambition of finding ways to improve the evacuation efficiency based upon changes in the room structure and the design of guidance schemes. The final category of research involves the flow of pedestrians in a T-shaped channel [16]–[22]; this kind of research focuses on the merging and separating behaviors of crowds of pedestrians in T-shaped channels. The merging behavior represents the movements of a crowd of pedestrians joining together from multiple directions to form a single streamline based on the same moving pedestrian target; by contrast, the separating behavior constitutes the movements of a crowd of pedestrians from a single streamline into two different directions based on different moving pedestrian targets. Researchers investigating the merging crowd behavior in a T-shaped channel obtain empirical data through organizing a series of controlled laboratory experiments to analyze the phase transformation mechanism and the cause of blockages during the merging process of pedestrian flow. As a result of these experiments, a series of basic graphs that reflect the macroscopic features of merging crowd behaviors in T-shaped channels and a large number of simulation models reflecting the interactions between pedestrians during the aggregation of pedestrian flows have been established. In our opinion, the research on the merging crowd behavior in a T-shaped channel is very mature.

Compared with the studies that have been reported on the merging crowd behavior, little research has been conducted on the separating crowd behavior in a T-shaped channel. When a pedestrian transitions from the main flow to one of the two destinations of the opposite branches in a distributary flow, conflicts between pedestrians and even congestion can arise. In the process of pedestrian separation, the individual decision-making mechanism and the interaction mode of pedestrians are also of great research value. In the existing research on the separating crowd behaviour in a T-shaped channel, the research performed by Fu *et al.* [21] is very representative, as it provides a valuable basis for subsequent research; in particular, they proposed a modified floor field cellular automaton (CA) model with a corresponding probability and studied the effect of the entrance density and the left-moving probability on the passing efficiency of pedestrians within a T-shaped channel through a simulation. In a follow-up study based on the research performed by Fu, Jia *et al.* considered the use of guide signage to improve the separation efficiency of pedestrian flow in a T-shaped channel and established a modified CA model considering the impact strength of the guide signage [22]. Nevertheless, the research on the separating crowd behavior in a T-shaped channel is still in its infancy due to a lack of support from controlled laboratory experiments and the fact that the simulation models lack validation with empirical data. In addition, the existing models do not fully consider the impacts of personality factors such as pedestrian preferences for swapping locations and their surroundings on the pedestrian decision-making process during the separating of pedestrian flow. These impacts cause certain deviations between the simulation results and real dynamic scenarios.

In our opinion, among the studies conducted heretofore on the simulation of pedestrian flow, relatively little simulation research has been performed on the separating crowd behavior in T-shaped channels, and even fewer simulation models have been developed with regard to the separating crowd behavior in T-shaped channels based on the social force model. In addition, the existing models also lack considerations of the differences in the walking habits of pedestrians and lack practical controllable experimental data to guide the simulation modeling. Consequently, we hope to contribute to this research field through the findings of this article. Here, we conduct a series of controlled experiments regarding the separating crowd behavior in a T-shaped channel, obtain experimental data on the walking trajectories and swapping locations of pedestrians moving during the process of separation. Based on the practical data, we propose an improved social force model to study the separating crowd behavior, and we analyze the influencing factors on the traffic efficiency within a T-shaped channel with the help of the improved model.

The key contributions of this paper are summarized as follows:

- We conduct a series of controlled experiments on the separating crowd behavior in a T-shaped channel. Based on the experimental results, the distribution of pedestrians' swapping locations moving during the process of separation is analyzed. We also make a comparison of the spatial and temporal distributions characteristics and macroscopic phenomena of pedestrians flow in two sets of controlled experiments in which the pedestrians' swapping locations are either dispersed or concentrated.
- Based on the data of real-world scenarios and pedestrians' behavior characteristics obtained by controllable experiments, we improve the social force model by refining the desired speed direction of each pedestrian. Our improved model fully considers the behavioral characteristics of pedestrians at different stages in the process of separation, and clearly reflects the influence of swapping location on pedestrians' movement.
- We conduct a series of simulation experiments regarding the separating crowd behavior in a T-shaped channel. The experimental results show that our improved model can well restore the motion characteristics of pedestrians in three different stages of the separation process in T-shaped channel. We also analyze the impact of the swapping location on the traffic efficiency in a T-shaped channel, and find ways to improve the traffic efficiency.

The remainder of this paper is organized as follows. In Section 2, we provide an overview of related work. In Section 3, we design controlled laboratory experiments regarding the separation of pedestrian flow within a T-shaped channel and obtain relevant empirical data. In Section 4, we revise the social force model to simulate the separating crowd behavior in a T-shaped channel. In Section 5, we verify the accuracy of the improved social force model and use the improved model to analyze the influencing factors on the evacuation efficiency of a separating pedestrian flow within a T-shaped channel. In Section 6, we conclude our work.

II. RELATED WORK

At present, there are many microscopic models that are suitable for simulation research on the moving behaviours of pedestrians. Overall, these models can be divided into two categories: discrete space models represented by lattice gas (LG) [23]–[25] and CA models [26]–[28] and continuous space models represented by the social force model [29]–[31] and VO-based (Velocity Obstacles) model [32]–[34].

Discrete space models divide the pedestrian space into small fixed cells and allow pedestrians to move at or within a fixed node or grid, and the pedestrian positions are updated at discrete time intervals [35]–[37]. In discrete space models, an approximate actual pedestrian behavior can be described by assigning simple rules to each individual, and the pedestrian movement rules can be intuitively represented by the probability of inhabiting a node or grid. This simple structure is known to be effective for reproducing collective phenomena observed in real pedestrian flow. Because of the discretization of both time and space, it is not necessary to use complex numerical methods to simulate the movements of pedestrians when using discrete space models; as a result, discrete space models exhibit a high simulation efficiency. However, some researchers have noted that the walking space in a discrete space model is discretized into square lattices, and thus, the choices for the speed and direction are limited; moreover, some drawbacks are encountered when representing multidirectional flow, especially for diagonal movements, and it is difficult to represent interactive cases in the real world [38]–[40].

In contrast to discrete space models, continuous space models such as the social force model [29], [30], [41] allow pedestrians to move continuously within a predefined geometry [7]; in addition, the speed of a pedestrian can be moved from 0 to the maximum continuously, and the movement directions in continuous space models are more flexible than those in discrete space models. Additionally, due to the continuity of the space, the social force model can effectively reproduce the interactions between the pedestrians and movement rules during a simulation of multidirectional pedestrian flow. Hence, the social force model constitutes a good, basic model for microscopic pedestrian simulations, but it is necessary to improve the social force when we restore the pedestrian walking rules or behavioral characteristics under some special conditions, and some practical factors need to be integrated into the model to improve the simulation accuracy, which cannot otherwise be guaranteed.

Follow-up simulation research has been carried out on more realistic dynamic scenarios by using the continually improving social force model. For instance, Helbing *et al.* [42] studied the herding behavior of pedestrians during a panicked situation in a smoky room; they considered the influence of the movement directions of surrounding pedestrians on their desired directions. In addition, Guo [12] studied the spatial and temporal separation of pedestrians moving in a counter flow through a bottleneck using the improved social force model and carefully defined the desired directions of the pedestrians, through which he described the spatial and temporal separation rules and moving characteristics of pedestrians within a counter flow moving through a narrow bottleneck; he also analyzed the effects of these separation rules on the traffic efficiency using the improved model. Furthermore, Yuan *et al.* used the improved social force model to study the crossing process of pedestrians in a bidirectional channel [43], [44] and proposed a new force model based on the social force model in consideration of individual moving preferences and following behaviors; subsequently, they used the improved model to study the merging and separation processes of pedestrian flow and analyzed the effects of individual and mass pedestrian behaviors on the self-organization of pedestrian flow.

Reciprocal Velocity Obstacles model (RVO model) proposed by Van Den Berg *et al.* [32], [33] is a kind of VO-based model for real-time multi-agent navigation. RVO model can simulate the collision-free motion of a large number of pedestrians in dense and complex scenes. Van Den Berg *et al.* introduced the concept of Velocity Obstacle to generate collision-free locomotion of agent based on velocity space sampling, transforms complex individual evacuation problems into low-dimensional linear planning problems, and in their simulation can add dynamic obstacles. Different from the social force model, the collision avoidance process is realized by the interaction force between pedestrians and pedestrians' desired speed are rarely changed, in the RVO model, the collision avoidance process between pedestrians is completely determined by the speed and available space between them. In order to prevent collisions between pedestrians, the new desired speed is calculated every time step, and the continuous new desired speed generated can ensure that pedestrians will not collide for a foreseeable time, resulting in a collision-free local navigation path. And different from the social force model, in the RVO model, the displacement and speed of the next time step do not need to be solved by complex numerical methods (e.g., the Euler method or the Runge-Kutta method), so the simulation efficiency of RVO model is more efficient than that of social force model.

There also exist many models based on agent simulation, in which motion trajectories are computed for each individual agent in a crowd [45]–[48]. The agent-based simulation model produces a detailed simulation result for each agent in the simulation for each simulation step. Each agent

represents a pedestrian in a real-life scene, the agent-based simulation model can perceive environmental information, such as obstacles and crowd distribution, and analyze the location of candidate path nodes, so that it can build a knowledge base of environmental information. In a recent study of agent-based simulation model, Luo *et al.* [48] identify two inter-related proactive steering behaviors, gap-seeking and following behaviors and proposed the detailed behavior models by considering the detected gap as a dynamic moving object. Their results show that the performance of the new agent-based model is better or at least comparable to the compared models(e.g. DS model [49]) in terms of the realism at both individual and crowd levels.

III. EXPERIMENTS

A. EXPERIMENTAL SETUP

Controlled experiments involving a separating pedestrian flow within a T-shaped channel were performed in a gymnasium in Changchun, China, in January 2018. A total of 60 participants (34 males and 26 females with a mean age of 20 years) were selected from different departments of the local institute. Referring to the preparation details of Shi *et al.* [19] for the setup of the experiment, some individual attributes of the participants were investigated. The average height of the male participants was 1.74 $\pm$ 0.1 m, and that of the female participants was 1.62 $\pm$ 0.12 m. Because the experiment was conducted in the winter, the participants were heavily dressed; the average shoulder width was 0.51 $\pm$ 0.03 m. The participants' individual desired walking speed (i.e., the average free walking speed) was $v_i^0(t) = 1.0$ m/s $\pm$ 0.2 m.

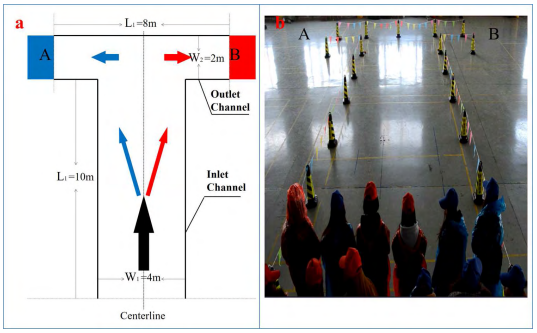

FIGURE 1. The experimental scenario of free motion.

As shown in Fig. 1, in the experimental scenario, the width of the inlet channel W_1 is 4 m, the length of the inlet channel L_1 is 10 m, the width of the outlet channel W_2 is 2 m, and the length of the outlet channel L_2 is 8 m. In the experiment, all of the participants entered from the entrance of the inlet channel with an average flow rate of 1.25 persons/m/s. The destination of the participants dressed in red with a red hat was exit B on the right side of the outlet channel, and the destination of the participants dressed in blue with a blue hat was exit A on the left side of the outlet channel. The numbers of red pedestrians and blue pedestrians were the same, and the positions of the red pedestrians and blue pedestrians entering the channel were random. Sixty participants walking within this limited space was sufficient to create a stable flow situation.

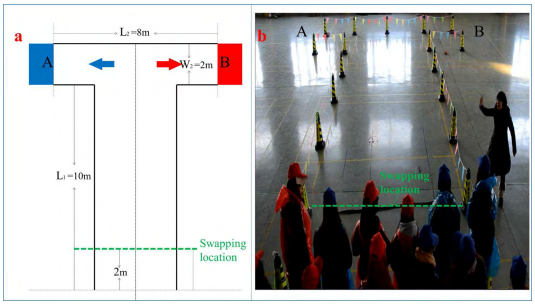

FIGURE 2. The experimental scenario of induced motion.

The controlled experiment consisted of two parts. In the first part, the participants moved freely 5 times in the scene shown in Fig. 1. In the second part, as shown in Fig. 2, we requested that the participants who were not on the same side of the inlet channel as their target direction to move through the pedestrian flow to the exit at a particular location; in other words, the blue pedestrians who were on the right side of the inlet channel were requested to move to the left side, and the red pedestrians who were on the left side of the inlet channel were requested to move to the right side to the same, concentrated position. In this experiment, the induced swapping location was set at 2 m from the entrance, and the experiment was repeated 5 times. As shown in Fig. 2.**a**, the green dotted line represents the induced swapping location, and Fig. 2.**b** shows a video screenshot of the experiment.

B. EXPERIMENTAL DATA ANALYSIS

First, we focused on the individual walking trajectories of pedestrians in free motion without induction. We choose two sets of representative motion trajectories for the analysis; their positions are taken every second starting from the time at which the pedestrians enter the channel. Fig. 3 shows a video screenshot of the movement of the blue pedestrian, and Fig. 4 shows a video screenshot of the movement of the red pedestrian. Fig. 5.**a** displays the walking trajectories of both types of pedestrians, where the red line is the red pedestrian's walking trajectory, and the blue line is the blue pedestrian's walking trajectory. We observe significant differences in their walking trajectories. The blue pedestrian consciously moves towards her/his destination (the left side of the outlet channel) upon initially entering the channel. After entering the inlet channel, there is a continuous leftward displacement in the trajectory of the blue pedestrian, and she/he passes through the center line of the inlet channel at a distance between 3 and 4 m from the entrance. In contrast to the blue pedestrian, the red pedestrian prefers to move initially along the direction of the inlet channel; at this stage, the walking trajectory of the red pedestrian is similar to a straight line. Then, the red pedestrian moves to the right side of the channel by passing the center line of the inlet channel at a distance

FIGURE 3. The video screenshots used to obtain the walking trajectories of the blue pedestrians.

FIGURE 4. The video screenshots used to obtain the walking trajectories of the red pedestrians.

between 6 and 7 m from the entrance. By comparing these trajectories, there are significant differences in the swapping locations of these two types of pedestrians.

Next, we collected the walking trajectories of all participants in the free movement experiment. As shown in Fig. 5.**b**, we find that the swapping locations of the pedestrians are not concentrated in a certain area; rather, due to the personality factors of the pedestrians, the swapping locations are scattered throughout the whole inlet channel. To research the pedestrians' swapping characteristics and crossing processes in a T-shaped channel, we use L_i to indicate a pedestrian's swapping location, that is, the initial position that produces a leftward or rightward displacement continuously in her/his walking trajectory. Taking the two pedestrians in Fig. 5.**a** as an example, the L_i of the red pedestrian is 3 m, and the L_i of the blue pedestrian is 0 m. As shown in Fig. 6, we analyze and count the L_i values of all participants in the 5 experiments and obtain the distribution of L_i accordingly. We discover that most pedestrians tend to move through the pedestrian flow to the exit at a distance of approximately 6 m from the entrance (77% of participants start changing lanes in the interval [0,6 m)); moreover, fewer pedestrians change their lanes the closer they are to the outlet channel (only 8% of participants change their lanes in the interval [8,10 m)).

To further analyze the impacts of the differences in the swapping location on the pedestrian flow in a T-shaped channel, we compared the experimental data before and after the induction. Fig. 7.**a** and Fig. 7.**b** are video screenshots of the free movement experiment; the time in Fig. 7.**a** is 10 seconds, and the time in Fig. 7.**b** is 20 seconds. Similarly, Fig. 7.**c** and Fig. 7.**d** are video screenshots of the induced movement experiment; the time in Fig. 7.**c** is 10 seconds, and the time in Fig. 7.**d** is 20 seconds. By comparing the video screenshots, the pedestrians are more dispersed

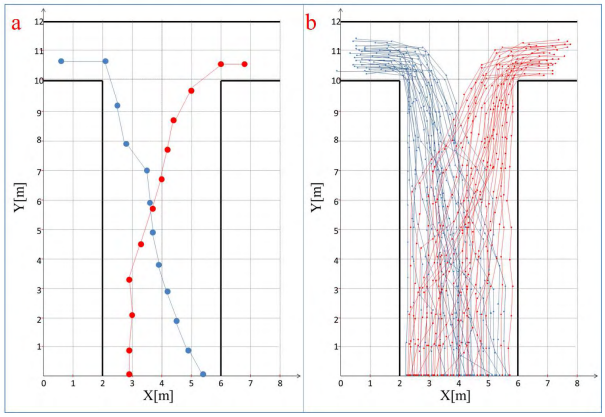

FIGURE 5. A comparison of the pedestrians' walking trajectories. (a) displays the walking trajectories of both types of pedestrians; (b) shows the walking trajectories of all participants in the free motion experiment.

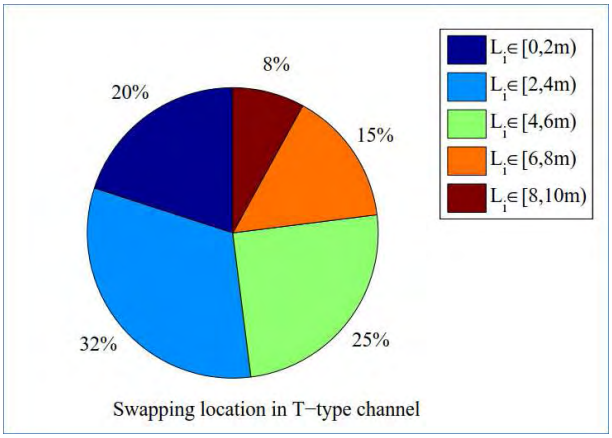

FIGURE 6. The distribution of the pedestrians' swapping locations.

throughout the inlet channel before the induction in the free movement experiment, and the locations of the two distributary flows are closer to the outlet channel. After the induction, the swapping locations of the pedestrians are limited to within a certain region, and the main flow from the induced swapping location is directly divided into two distributary flows. This difference in the macroscopic phenomena becomes more apparent during the walking process. As shown in Fig. 7.**b**, when the duration of the free movement experiment reaches 20 seconds, the pedestrians are still changing lanes in the middle of the inlet channel. In contrast, as shown in Fig. 7.**d**, when the duration of the induced movement experiment reaches 20 seconds, two distinct distributary flows have formed within the channel, and almost all of the pedestrians have completed the process of changing lanes.

We also compared the spatial and temporal distribution characteristics of the pedestrians in the free movement and the induced movement experiments. As shown in Fig. 8, we record the variations in the numbers of pedestrians with both time and space in the left half of the T-shaped channel. Fig. 8.**a** and Fig. 8.**b** represent the changes in the number of blue pedestrians and red pedestrians, respectively, in the free movement experiment, while Fig. 8.**c** and Fig. 8.**d** represent the changes in the number of blue pedestrians and red pedestrians, respectively, in the induced movement experiment. As shown in Fig. 8, due to the random locations of the pedestrians entering the inlet channel, no obvious difference in the quantities of blue pedestrians and red pedestrians is observed at the entrance of the channel (channel lengths between 0 m and 2 m) at the beginning of the free movement experiment. However, during the course of the experiment, since the blue pedestrians' destination is the left side of the outlet channel, the blue pedestrians gradually move towards the left side of the inlet channel, and the number of blue pedestrians on the left side of the channel increases significantly beyond the number of red pedestrians. When the experiment reaches 20 seconds, only a few (i.e., 1 or 2) red pedestrians are still within the channel at distances between 6 and 10 m, and the outlet channel (channel lengths between 10 m and 12 m) is entirely inhabited by blue pedestrians. During the induced movement experiment, the numbers of blue pedestrians and red pedestrians change faster than those in the free movement experiment; moreover, when the induced experiment reaches 17 seconds, no red pedestrians are within the channel between 4 and 12 m. In addition, comparing the average times used in the two sets of experiments, the duration of the free movement experiment is 34 seconds, and the duration of the induced movement experiment is 32 seconds.

This series of controlled experiments provides the following important implications:

1. There are obvious differences in the swapping locations of pedestrians in a T-shaped channel. Therefore, during simulation modeling, we need to design attributes for each pedestrian to reflect these differences in the swapping locations.
2. Different swapping locations can generate different macroscopic phenomena, and differences in the spatial and temporal distributions of pedestrian flow will also cause variations in the traffic efficiency within a T-shaped channel. We can thus use induction to change the swapping locations within the pedestrian flow so that the flow can be moved more efficiently, thereby improving the traffic efficiency in a T-shaped channel.

In the following work, we will construct a new simulation model that considers the differences in the swapping location based on the social force model; then, through simulation experiments, we will analyze how the swapping location affects the channel traffic efficiency and find ways to improve the traffic efficiency within a T-shaped channel.

IV. MODEL

The social force model for pedestrian flow is as follows [42]:

$$m_i \frac{d\mathbf{v}_i}{dt} = \mathbf{f}_{will} + \sum_{j(\neq i)} \mathbf{f}_{ij} + \sum_{W} \mathbf{f}_{iw} \tag{1}$$

$$\mathbf{f}_{will} = m_i \frac{v_i^0(t)\mathbf{e}_i^0(t) - v_i(t)}{\tau_i} \tag{2}$$

FIGURE 7. A comparison of the video screenshots before and after the induction.

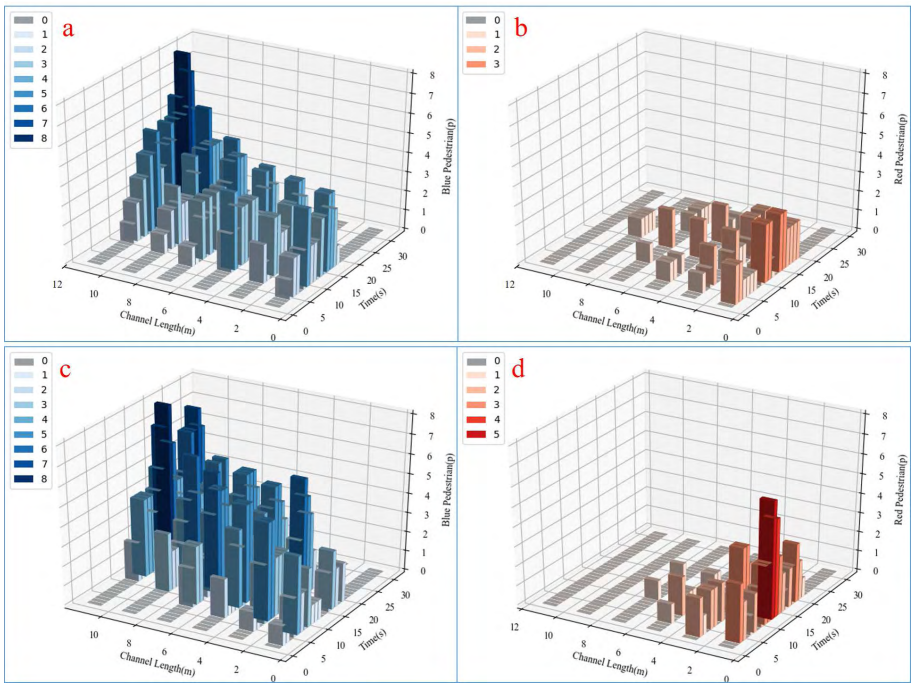

FIGURE 8. Comparison of the spatial and temporal distributions of pedestrians before and after the induction.

In the social force model, the movement of a pedestrian is affected by three types of forces: the will force $\mathbf{f}_{will}$ that reflects the influence of a moving target on the pedestrian, the interaction force $\mathbf{f}_{ij}$ between a pedestrian and nearby pedestrians, and the interaction force $\mathbf{f}_{iw}$ between a pedestrian and nearby walls or obstacles.

The equation (2) for the will force $\mathbf{f}_{will}$ indicates that a pedestrian i of mass m_i likes to move at a certain desired speed v_i^0 in a certain direction $\mathbf{e}_i^0$, which is generally the destination direction; therefore, a pedestrian tends to correspondingly adapt her/his actual velocity $\mathbf{v}_i$ with a certain characteristic time τ_i. The function of $\mathbf{f}_{will}$ enables a pedestrian to achieve her/his desired speed v_i^0 and to shift her/his actual direction of motion towards her/his destination direction $\mathbf{e}_i^0$. However, the direction of $\mathbf{f}_{will}$ is not the destination direction; rather, the direction is $v_i^0(t)\mathbf{e}_i^0(t) - \mathbf{v}_i(t)$, which shows

that the actual effect of this force represents a corrective action.

The change in the movement speed of a pedestrian is influenced by not only the will force but also the interaction forces $\sum_{j(\neq i)} \mathbf{f}_{ij}$ and $\sum_{W} \mathbf{f}_{iw}$. A pedestrian i tends to maintain a velocity-dependent distance from another pedestrian j and from walls W. To include this tendency, the interaction forces $\mathbf{f}_{ij}$ and $\mathbf{f}_{iw}$ are added into the social force model as follows:

$$\begin{aligned}\mathbf{f}_{ij} = &\{A_i exp[(r_{ij} - d_{ij})/B_i] + kg(r_{ij} - d_{ij})\}\mathbf{n}_{ij} \\ &+ \kappa g(r_{ij} - d_{ij})\Delta v_{ji}\mathbf{t}_{ij}\end{aligned} \tag{3}$$

where A_i and B_i are positive constants, r_{ij} is the sum of the radii r_i and r_j, $d_{ij} = \|d_i - d_j\|$ denotes the distance between the centers of two pedestrians, $\mathbf{n}_{ij}$ is the unit vector pointing from pedestrian j to i, and $\mathbf{t}_{ij}$ is a tangential direction. The function $g(x)$ equals zero if the pedestrians do not touch each other ($d_{ij} > r_{ij}$) and otherwise equals the argument x.

$$\begin{aligned}\mathbf{f}_{iw} = &\{A_i exp[(r_i - d_{iw})/B_i] + kg(r_i - d_{iw})\}\mathbf{n}_{iw} \\ &+ \kappa g(r_i - d_{iw})(\mathbf{v}_i \cdot \mathbf{t}_{iw})\mathbf{t}_{iw}\end{aligned} \tag{4}$$

where A_i and B_i are positive constants, d_{iw} denotes the distance between a wall and pedestrian i, $\mathbf{n}_{iw}$ is the unit vector pointing from the wall to pedestrian i, and $\mathbf{t}_{iw}$ is a tangential direction. The function $g(x)$ equals zero if the pedestrians do not touch the wall ($d_{iw} > r_i$) and otherwise equals the argument x.

The change in the position $\mathbf{p}_i(t)$ at time t is determined by the following velocity equation:

$$\frac{d\mathbf{p}_i(t)}{dt} = \mathbf{v}_i(t) \tag{5}$$

By using Euler's method, the velocity and the position of pedestrian i are updated at each time step Δt with the following system of equations:

$$\mathbf{v}_i(t + \Delta t) = \mathbf{v}_i(t) + \frac{d\mathbf{v}_i(t)}{dt}\Delta t \tag{6}$$

$$\mathbf{p}_i(t + \Delta t) = \mathbf{p}_i(t) + \mathbf{v}_i(t)\Delta t + \frac{1}{2}\frac{d\mathbf{v}_i(t)}{dt}\Delta t^2 \tag{7}$$

In the social force model, $\mathbf{f}_{ij}$ and $\mathbf{f}_{iw}$ reflect the passive behaviors of pedestrians when their free movement is limited, and $\mathbf{f}_{will}$ reflects the willingness of pedestrians to walk according to their own initiative. In the $\mathbf{f}_{will}$ model, the desired direction $\mathbf{e}_i^0(t)$ can significantly affect both the movement pattern and the walking trajectory. However, the present study lacks an actual investigation into the characteristics of pedestrians' swapping and crossing locations; because the swapping location is subjectively confined to a region close to the outlet channel, research based on the swapping location will be biased against reality. To replicate the actual situation of separating crowd behavior, we introduce the parameter L_i, which reflects the pedestrian transposition personality factor, into the social force model to refine the desired direction $\mathbf{e}_i^0(t)$ shown in (8), as shown at the bottom of this page.

Where L_1 and W_1 are the length and width, respectively, of the inlet channel, L_2 and W_2 are the respective length and width of the outlet channel, r_i is the radius of pedestrian i, $p_i^x(t)$ and $p_i^y(t)$ are the components of the pedestrian displacement $\mathbf{p}_i(t)$ along the X and Y axes, respectively, and $L_i \in [0, L_1]$ is a characteristic parameter reflecting the pedestrian's swapping location. Formula (8) reflects the change in the desired direction ($\mathbf{e}_i^0(t)$) with the position of the pedestrian ($\mathbf{p}_i(t)(p_i^x(t), p_i^y(t))$) whose destination is the left side of the outlet channel (i.e., the blue pedestrian in the controlled experiment). As shown in Fig. 9**a**, Formula (8) indicates that the change in the desired direction can be divided into three stages. In the first stage, the pedestrian walks along the direction of the inlet channel, and pedestrians who are not

$$\mathbf{e}_i^0(t) = \begin{cases} \dfrac{(p_i^x(t), L_1) - \mathbf{p}_i(t)}{\|(p_i^x(t), L_1) - \mathbf{p}_i(t)\|} & \frac{1}{2}(L_2 - W_1) + r_i < p_i^x(t) < \frac{1}{2}(L_2 - W_1) + W_1 - r_i \text{ and } p_i^y(t) < L_i + r_i \\ \dfrac{(\frac{1}{2}(L_2 - W_1), L_1 + \frac{1}{2}W_2) - \mathbf{p}_i(t)}{\|(\frac{1}{2}(L_2 - W_1), L_1 + \frac{1}{2}W_2) - \mathbf{p}_i(t)\|} & \frac{1}{2}(L_2 - W_1) + r_i < p_i^x(t) < \frac{1}{2}(L_2 - W_1) + W_1 - r_i \text{ and } L_i + r_i \leq p_i^y(t) < L_1 + r_i \\ \dfrac{(0, p_i^y(t)) - \mathbf{p}_i(t)}{\|(0, \mathbf{p}_i^y(t)) - \mathbf{p}_i(t)\|} & \text{otherwise} \end{cases} \tag{8}$$

$$\mathbf{e}_i^0(t) = \begin{cases} \dfrac{(p_i^x(t), L_1) - \mathbf{p}_i(t)}{\|(p_i^x(t), L_1) - \mathbf{p}_i(t)\|} & \frac{1}{2}(L_2 - W_1) + r_i < p_i^x(t) < \frac{1}{2}(L_2 - W_1) + W_1 - r_i \text{ and } p_i^y(t) < L_i + r_i \\ \dfrac{(\frac{1}{2}(L_2 + W_1), L_1 + \frac{1}{2}W_2) - \mathbf{p}_i(t)}{\|(\frac{1}{2}(L_2 + W_1), L_1 + \frac{1}{2}W_2) - \mathbf{p}_i(t)\|} & \frac{1}{2}(L_2 - W_1) + r_i < p_i^x(t) < \frac{1}{2}(L_2 - W_1) + W_1 - r_i \text{ and } L_i + r_i \leq p_i^y(t) < L_1 + r_i \\ \dfrac{(L_2, p_i^y(t)) - \mathbf{p}_i(t)}{\|(L_2, p_i^y(t)) - \mathbf{p}_i(t)\|} & \text{otherwise} \end{cases} \tag{9}$$

TABLE 1. Parameters in this simulation.

symbol	meaning	value
v_i^0	desired speed	1.0 m/s
m_i	pedestrian mass	65 kg
τ_i	characteristic time	0.1 s
r_i	pedestrian radius	0.25 m
A_i	avoidance force intensity	25 ms^{-2}
B_i	avoidance coefficient	0.08 m
k	body force coefficient	1500 kg/s^2
κ	friction force coefficient	3000 $kg/(m \cdot s)$
Δt	time step	5×10^{-3} s
P_{in}	flow rate at the entrance	[0.25, 2.5 persons/m/s]
L_i	characteristic parameter reflecting the swapping location	[0,10 m]
L_1	length of the inlet channel	10 m
W_1	width of the inlet channel	4 m
L_2	length of the outlet channel	8 m
W_2	width of the outlet channel	2 m

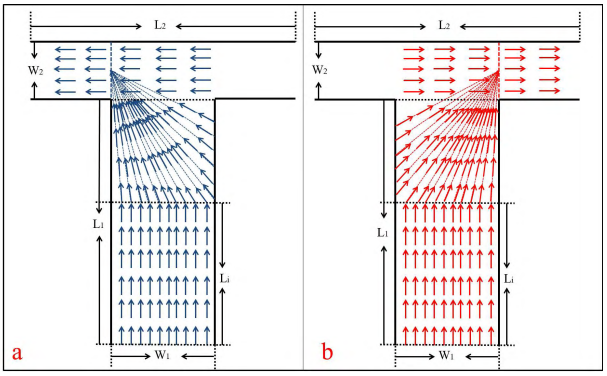

FIGURE 9. The changes in the pedestrians' desired directions.

affected by other pedestrians will not produce a significant leftward or rightward displacement. In the second stage, after the pedestrian walks to a specific position $L_i \in [0, L_1]$, she/he begins to adjust her/his movement direction to consciously move towards the left side of the outlet channel. In the third stage, after the pedestrian enters the outlet channel, her/his desired direction is towards the left exit (−1,0 m). Similarly, as shown in Fig. 9**b** for each pedestrian i whose moving target is towards the right side of the outlet channel (i.e., the red pedestrians in the controlled experiment), the desired direction $\mathbf{e}_i^0(t)$ is computed by Formula (9), as shown at the bottom of the previous page. Using the above formula, we can set the swapping position for each pedestrian so that the distribution of swapping locations within the pedestrian flow can be established according to the proportion obtained by the controlled experiment; we can also set the swapping positions of all pedestrians within a certain range so that a simulation analysis of the induced movement experiment can be performed. Accordingly, it is also possible to study the effect of the degree of convergence of the swapping position on the traffic efficiency within a T-shaped channel.

In addition to this, we have to explain that the purpose of our model is to be able to fully consider the differences in pedestrians' swapping location in the simulation, of course, this is not the only way to achieve this goal, the swapping locations and target locations can be determined as the way points by the path planer and the agents navigate to these way points with the original social force model in the agent-based simulation for T-shaped Channel. The computing method of these way points can also refer to the formulas we put forward above. Under the same parameters and experimental design, the simulation results will be the same.

V. SIMULATION AND DISCUSSION

Referring to the experimental data and the research of Guo [12], we take the parameters shown in Table 1 for the simulation.

In this section, we will describe some phenomena and qualitative results through simulating the movement processes of pedestrians in the scenarios shown in Fig. 1 and Fig. 2 by applying the improved social force model. The size of the area is defined as follows: the width of the inlet channel W_1 is 4 m, the length of the inlet channel L_1 is 10 m, the width of the outlet channel W_2 is 2 m, and the length of the outlet channel L_2 is 8 m.

First, we illustrate that the improved social force model can reflect the impact of the swapping location on the movement process of pedestrians. We use the Longest Common Subsequence (LCSS) metric for evaluating the trajectory similarity between the ground truth trajectory and simulated trajectory. In the simulation experiments, the flow rate at the entrance, the positions at which pedestrians enter the channel is the same as that in the controlled experiment. The LCSS metric is efficient techniques to accurately compute the similarity between trajectories of moving objects [48], [50], [51]. The LCSS similarity metric is calculated as Equation(10).

$$S_{LCSS}(Tr^{real}, Tr^{sim}) = \frac{LCSS(Tr^{real}, Tr^{sim})}{min(m, n)} \tag{10}$$

where $Tr^{real} = ((a_{x,1}, a_{y,1}), ...(a_{x,n}, a_{y,n}))$ and $Tr^{sim} = ((b_{x,1}, b_{y,1}), ...(b_{x,n}, b_{y,m}))$ are ground truth trajectory and simulated trajectories with size m and n respectively. $LCSS(Tr^{real}, Tr^{sim})$ is define as Equation (11), as shown at the bottom of the next page. In Equation (11), δ is a user-defined

integer which controls how far in time we can go in order to match a given point from the ground truth trajectory to a point in simulated trajectory, the user-defined constant $0 < \varepsilon < 1$ is the matching threshold, $Head(Tr^{real})$ and $Head(Tr^{sim})$ are the first points in trajectory Tr^{real} and Tr^{sim} respectively, $d_E(a_n - b_m)$ is the Euclidean distance between the *nth* point in Tr^{real} and *mth* point Tr^{sim}. This similarity function is based on the LCSS and the idea is to allow time stretching. Then, objects that are close in space at different time instants can be matched if the time instants are also close [50]. Referring to the research of Luo *et al.* [48], we set $\delta = 20\%$ and $\varepsilon = 0.4$ for LCSS, and select 30 pedestrians' trajectories for evaluating, in order to ensure the universality of similarity analysis, there are differences in these pedestrians' swapping locations. We obtain the average S_{LCSS} in 20 independent simulations. The average S_{LCSS} in our improved social force model which considering the differences of swapping locations is 74.16 ± 2.13, we can also find that if we make all the pedestrians' swapping locations concentrated in a certain range in the simulation without considering the differences of swapping locations the S_{LCSS} will be much reduced, for example, if we make all the pedestrians' L_i equal to 6m, the S_{LCSS} is 32 ± 1.07, and if L_i equal to 8m the S_{LCSS} is only 21.65 ± 1.51.

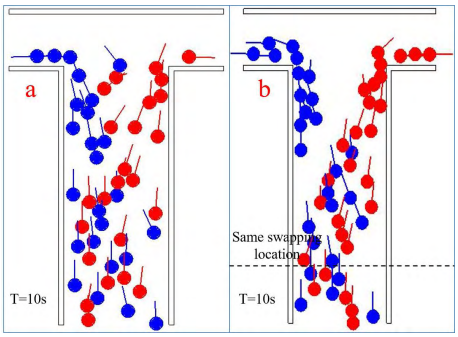

FIGURE 10. A comparison of the screenshots obtained between both sets of simulation experiments.

We also analyzed the effect of swapping location on the separating crowd behaviour in a T-shaped Channel from a microscopic perspective. In the simulation experiments, the flow rate at the entrance is the same as that in the controlled experiment, the proportion of pedestrians in different destinations is the same, and the positions at which pedestrians enter the channel are random. In Fig. 10, the blue circles represent the pedestrians whose destination is the left side of the outlet channel, while the red circles represent the pedestrians whose destination is the right side of the outlet channel, and the short lines extruding from the circles represent the movement directions of the pedestrians. In Fig. 10.**a**, the swapping locations of the pedestrians are dispersed, and the distribution of swapping locations L_i is consistent with that shown in Fig. 6; in contrast, in Fig. 10.**b**, the swapping locations of all pedestrians are concentrated (L_i is 2 m). From a microscopic perspective, the separation behavior of pedestrians is dispersed throughout the inlet channel in Fig. 10.**a**, and some red or blue pedestrians are still starting to adjust their movement directions to their corresponding destinations near the outlet channel. In Fig.10.**b**, all of the pedestrians are beginning to adjust their movement directions after passing the swapping location in advance; furthermore, there are almost no red pedestrians on the left side of the inlet channel near the outlet channel, and similarly, there are no blue pedestrians on the right side of the inlet channel. From a macroscopic perspective, at the same time, the two distributary flows shown in Fig. 10.**a** are not as obvious as those in Fig. 10.**b**; in Fig. 10.**b**, the pedestrians are more concentrated within the distributary flows. These findings are in accordance with the phenomena we observed in the controlled experiments.

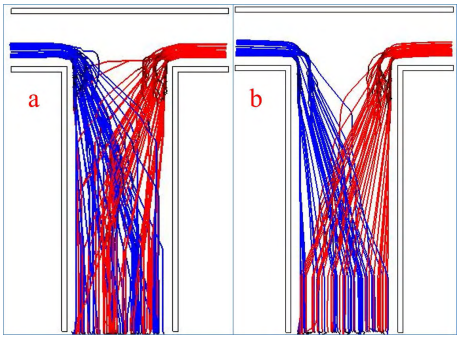

FIGURE 11. A comparison of the pedestrians' moving trajectories between both sets of simulation experiments. In Fig. 11.a, the swapping locations of the pedestrians are different; in Fig. 11. b, the swapping locations of the pedestrians are the same.

We also obtained the pedestrians' moving trajectories in both sets of simulation experiments. In Fig. 11.**a**, the swapping locations of the pedestrians are dispersed; in contrast, in Fig. 11.**b**, the swapping locations of the pedestrians are concentrated. There are significant differences in the pedestrian trajectories between the two sets of simulation experiments; the pedestrian trajectories in Fig. 11.**a** are closer to the pedestrians' moving trajectories obtained in the controlled experiment shown in Fig. 5.**b**. These results also verify the necessity and feasibility of our improved model.

Next, we analyzed the impact of the swapping location on the traffic efficiency in a T-shaped channel. In these simulation experiments, we use a continuously increasing flow rate at the entrance P_{in}, and the size of the experimental area is the

$$\begin{cases} 0 & \text{if } Tr^{real} \text{ or } Tr^{sim} \text{ is empty} \\ 1 + LCSS_{\delta,\varepsilon}(Head(Tr^{real}), Head(Tr^{sim})) & d_E(a_n - b_m) < \varepsilon \text{ and} n - m < \delta \\ max(LCSS_{\delta,\varepsilon}(Head(Tr^{real}), Tr^{sim}), LCSS_{\delta,\varepsilon}(Tr^{real}, Head(Tr^{sim}))) & \text{otherwise} \end{cases} \quad (11)$$

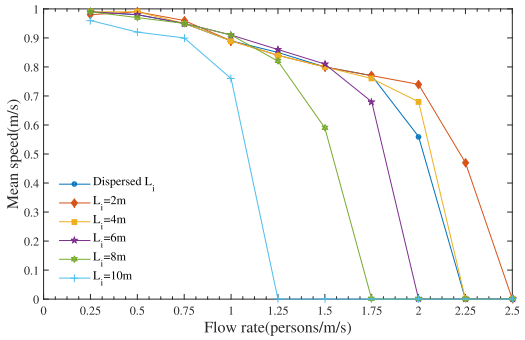

FIGURE 12. The fundamental diagram of the simulation experiments.

same as that in the previous simulation experiment. Similarly, the simulation experiment is divided into two sets. In the first set, we assume that the swapping locations of the pedestrians are also dispersed under different flow rate conditions, and the distribution of the swapping locations L_i is consistent with that shown in Fig.6. In the second set, we assume that the swapping locations of all pedestrians are concentrated, and we set the concentrated swapping locations as $L_i = 2$ m, 4 m, 6 m, 8 m,and 10 m. The simulation results are averaged over 20 independent simulations. The fundamental diagram of the simulation experiments is shown in Fig. 12, which demonstrates that the mean speeds of the pedestrians in both sets of simulation experiments decrease with an increase in the flow rate at the entrance; however the flow rates that generate congestion (mean speed=0 m/s) in each experiment are not the same. In the first set of simulation experiments, when the flow rate at the entrance P_{in} is 2.25 persons/m/s, congestion occurs in the T-shaped channel. In the second set of simulation experiments, the swapping locations L_i are concentrated; when $L_i = 2$ m, 4 m, 6 m, 8 m, and 10 m, the thresholds of the flow rate are 2.5 persons/m/s, 2.25 persons/m/s, 2 persons/m/s, 1.75 persons/m/s, and 1.25 persons/m/s, respectively. In the second set of simulation experiments, the closer the concentrated swapping location L_i is to the entrance, the higher the mean speed; moreover, if the concentrated swapping location L_i is relatively close to the outlet channel ($L_i = 8$ m or 10 m), the traffic efficiency in the T-shaped channel is low, even under relatively small flow rate conditions. Comparing both sets of experiments, the traffic efficiency in the T-shaped channel is better in the second set of simulation experiments than in the first set when the concentrated swapping location L_i is either 2 m or 4 m and the flow rate at the entrance $P_{in} \geq 2$ persons/m/s; however, when the concentrated swapping location $L_i \geq 4$ m, the traffic efficiency within the T-shaped channel in the first set of simulation experiments is better than that in the second set. The simulation results also remind us that as the flow rate at the entrance increases, the influence of the swapping location on the traffic efficiency in the T-shaped channel becomes gradually enhanced. In addition, the closer the pedestrians' swapping location is to the outlet channel, the lower the traffic efficiency within the T-shaped channel; in contrast, the closer the pedestrians' swapping location is to the entrance, the higher the traffic efficiency in the T-shaped channel.

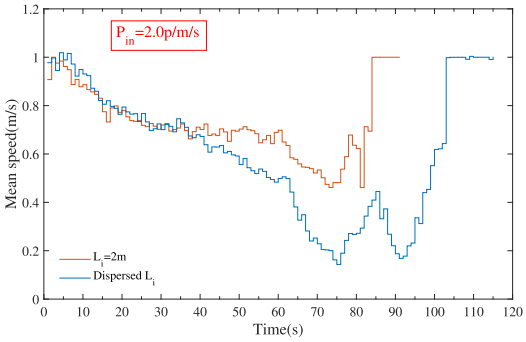

FIGURE 13. A plot of the mean speed versus the time.

To study the effect of the swapping location on the traffic efficiency within the T-shaped channel, we also compared the changes in the mean speeds in both sets of simulation experiments. In the simulation, the flow rate at the entrance P_{in} is 2 persons/m/s, and the time to generate pedestrians is 60 seconds; the results are shown in Fig. 13. Evidently, the completion time of the simulation with a dispersed swapping location L_i is 25 seconds longer than that of the simulation with $L_i = 2$ m; furthermore, the mean speed in the simulation with a dispersed swapping location L_i is substantially lower than that in the simulation with a concentrated swapping location $L_i = 2$ m after 38 seconds. In addition, the change in the mean speed during the simulation with $L_i = 2$ m is more stable that those during the simulations with dispersed values of L_i, and the range of changes in the mean speed in the simulation with dispersed values of L_i is greater than that in the simulation with $L_i = 2$ m.

To further explore the reasons why the swapping location affects the traffic efficiency in a T-shaped channel, we compared the simulation screenshots at the same time. According to the previous simulation results, different congestion conditions will be observed during the simulation with a flow rate at the entrance of $P_{in} = 2$ persons/m/s. Fig. 14.**a** shows a screenshot of the simulation in which the pedestrians' swapping locations are dispersed; in Fig. 14.**b** through Fig. 14.**f**, the swapping locations are concentrated, and the concentrated swapping locations L_i are 2 m, 4 m, 6 m, 8 m, and 10 m. Comparing Fig. 14.**a** with Fig. 14.**b**, the former demonstrates that there are significant conflicts between the pedestrians in the area despite the absence of complete congestion within the T-shaped channel, and some red/blue pedestrians are forced to go to the opposite sides of their corresponding destinations in the outlet channel (the parts of the figure denoted by dotted circles). In Fig. 14.**b**, there are fewer conflicts among the pedestrians, and two distributary flows have formed before the pedestrians begin entering the outlet channel; thus, no pedestrians are forced to move towards the opposite side of her/his destination in the outlet channel.

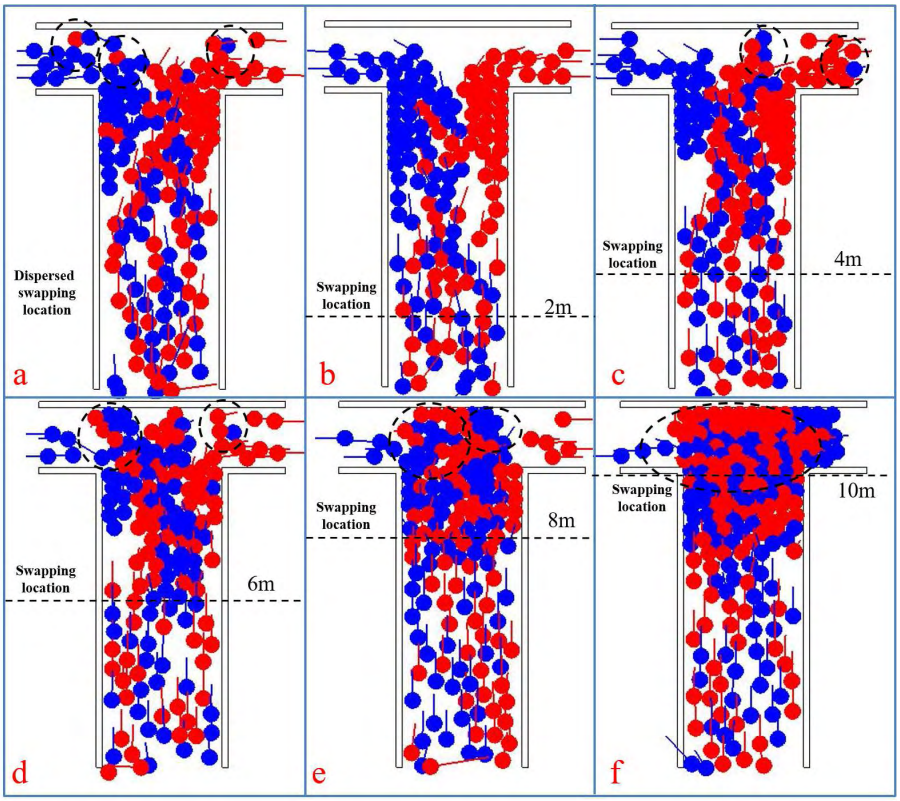

FIGURE 14. A comparison of simulation screenshots. With dispersed swapping location for pic.(a) and concentrated L_i = 2m, 4m, 6m, 8m, and 10m for others, respectively.

A comparison of the screenshots of the experiments in which the swapping locations of all pedestrians are concentrated shows that the range of conflicts among pedestrians grows as the lag in the swapping location increases; moreover, when the pedestrians' swapping locations are closer to the entrance, the formation of distributary flows is more favorable, and there are fewer conflicts between pedestrians.

To further corroborate our assertion that we can reduce conflicts between pedestrians by adjusting the swapping location, we analyzed the number of conflicts among pedestrians under different flow rates at the entrance; the time used to count the number of conflicts is 60 seconds. In this article, a conflict is defined by physical contact between two pedestrians with opposite destinations. Fig. 15 shows the simulation results regarding the number of conflicts between pedestrians throughout the T-shaped channel. Overall, as the flow rate at the entrance increases, the number of pedestrian conflicts increases in every set of simulation experiments, but there are still significant differences in the number of conflicts among the different simulation sets. Comparing the number of conflicts in the simulation with dispersed swapping locations with those in the simulations with concentrated swapping locations, the number of conflicts in the simulation with a dispersed swapping location is higher than that in the simulation with $L_i = 2$ m, and this difference becomes increasingly obvious with an increase in the channel flow rate; when the

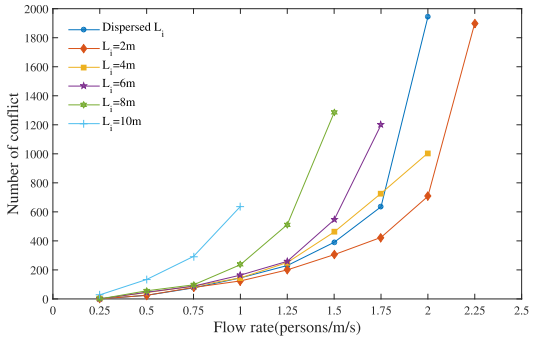

FIGURE 15. The number of conflicts between pedestrians under different flow rates at the entrance.

flow rate at the entrance is $P_{in} = 2$ persons/m/s, the number of conflicts in the simulation with $L_i = 2$ m is 707, and that in the simulation with dispersed swapping locations is 1943. Upon comparing the numbers of conflicts in the simulations with concentrated swapping locations, we discover that fewer conflicts occur when the pedestrians' swapping locations are closer to the entrance under the same flow rate at the entrance. Moreover, the number of conflicts increases with later lags in the swapping location; for instance, the number of conflicts in the simulation with $L_i = 10$ m is 637, and that in the simulation with $L_i = 2$ m is only 124 when the flow rate is $P_{in} = 1$ persons/m/s.

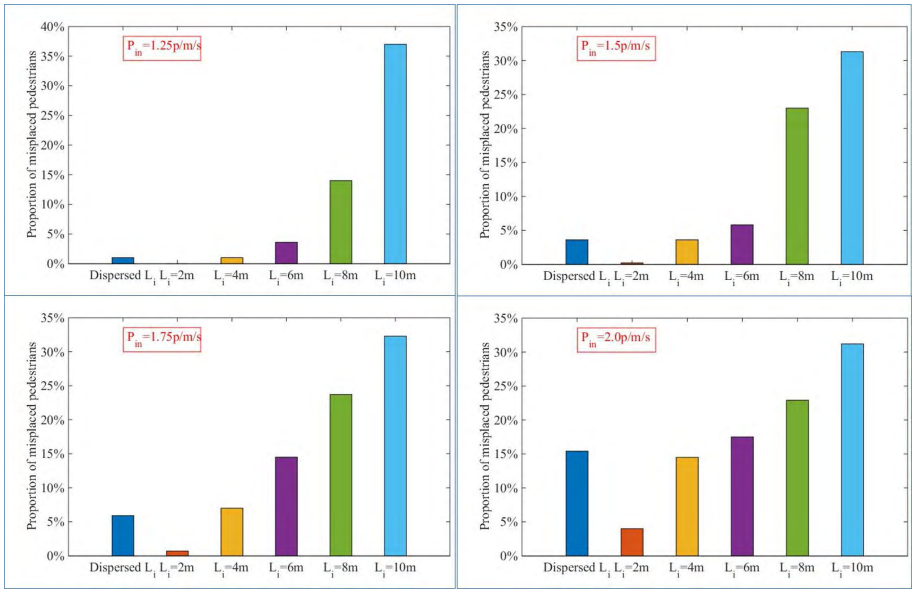

FIGURE 16. Proportion of misplaced pedestrians under different flow rates at the entrance.

We also analyzed the situations in which the pedestrians are forced to move towards the side of the channel opposite their outlet channel destinations. Examining the simulation screenshots reveals that some red/blue pedestrians are forced to move towards the side of the channel opposite their outlet channel destination (the pedestrians in the parts of Fig. 14 denoted by dotted circles). When such misplaced pedestrians move towards their own destination, they inevitably collide with other pedestrians moving in the opposite direction; we consider this situation to be the main cause of congestion in the T-shaped channel, and thus, we counted the proportion of misplaced pedestrians. The method used to count the number of misplaced pedestrians is as follows: if a pedestrian walks towards the side of the channel opposite her/his destination, we regard such a pedestrian as a misplaced pedestrian. In the simulations, we counted misplaced pedestrians for 60 seconds under different flow rates at the entrance; the results are shown in Fig. 16. Before reaching the flow rate that generates congestion, the proportions of misplaced pedestrians increase in every simulation set as the flow rate at the entrance P_{in} increases. The proportion of misplaced pedestrians in the simulation with dispersed L_i is higher than that in the simulation with $L_i = 2$ m under different flow rates at the entrance; for example, the proportion of misplaced pedestrians in the simulation with dispersed L_i reaches 15.4% when the flow rate at the entrance is $P_{in} = 2$ persons/m/s, and the proportion in the simulation with $L_i = 2$ m is only 4%. Furthermore, similar to the situation involving conflicts between pedestrians, the closer the pedestrians' swapping location L_i is to the entrance, the lower the proportion of misplaced pedestrians under the same flow rate at the entrance; for example, there are no misplaced pedestrians in the simulation with $L_i = 2$ m, but the proportions in the simulations with $L_i = 8$ m and 10 m are 14% and 37%, respectively, when the flow rate at the entrance is $P_{in} = 1.25$ persons/m/s. An increase in the number of misplaced pedestrians will exacerbate the conflicts between pedestrians in a T-shaped channel; concentrating the pedestrians' swapping locations and moving the swapping locations closer to the entrance can help pedestrian flows complete the separation process earlier, thereby reducing the proportion of misplaced pedestrians and the number of conflicts between pedestrians.

VI. CONCLUSIONS

I. We conducted a series of controlled experiments on the separating crowd behavior in a T-shaped channel. The experimental results show that pedestrians' swapping locations are dispersed in the inlet channel rather than concentrated in a certain area. We also find significant differences in the macroscopic phenomena and spatial and temporal distribution characteristics of pedestrians in two sets of controlled experiments in which the pedestrians' swapping locations are either dispersed or concentrated.

II. We proposed an improved social force model for the separating crowd behavior in a T-shaped channel that fully considers the characteristics of pedestrians' swapping locations and refines the directions of pedestrians' expected speeds in three stages of the pedestrian separation process. Confirmed by simulation experiments, this improved model can effectively reflect the differences in pedestrians' separating behaviors, and a simulation result obtained in the controlled experiment shows that applying the improved model replicates the pedestrians' moving trajectory.

III. We conducted a series of simulation experiments regarding the separating crowd behavior in a T-shaped channel. The experimental results show that if pedestrians' swapping

locations are concentrated in a certain area that are relatively close to entrance, the traffic efficiency in the T-shaped channel will be higher than that if the pedestrians' swapping locations are dispersed. Furthermore, as the flow rate at the entrance increases, the swapping location becomes more concentrated and closer to the entrance, the mean speed becomes higher, and fewer conflicts occur between pedestrians.

In future work, we will study the influences of other factors, for example, the size of the channel and the herding behavior, on the traffic efficiency within a T-shaped channel. Moreover, we will carry out more controllable experiments on pedestrian flow to accumulate video data for different sports scenarios, and we hope to calibrate the parameters in the social force model and improve the model. In order to expand our research ideas, we also want to carry out simulation research based on multi-agent model and RVO-based model, and extend our existing research content to the field of multi-agent based simulation research.

ACKNOWLEDGMENTS

The authors would like to thank Dr. Wang (Weixi Wang) for the stimulating discussions.

REFERENCES

[1] M. Moussaïd, D. Helbing, and G. Theraulaz, "How simple rules determine pedestrian behavior and crowd disasters," *Proc. Nat. Acad. Sci. USA*, vol. 108, no. 17, pp. 6884–6888, 2011.

[2] G. D. Tian, H. H. Zhang, Y. X. Feng, D. Q. Wang, Y. Peng, and H. F. Jia, "Green decoration materials selection under interior environment characteristics: A grey-correlation based hybrid MCDM method," *Renew. Sustain. Energy Rev.*, vol. 81, pp. 682–692, Jan. 2018.

[3] J. Ma, W.-G. Song, J. Zhang, S.-M. Lo, and G.-X. Liao, "k-nearest-neighbor interaction induced self-organized pedestrian counter flow," *Phys. A, Stat. Mech. Appl.*, vol. 389, no. 10, pp. 2101–2117, 2010.

[4] H. Yue, H. Guan, J. Zhang, and C. Shao, "Study on bi-direction pedestrian flow using cellular automata simulation," *Phys. A, Stat. Mech. Appl.*, vol. 389, no. 3, pp. 527–539, 2010.

[5] J. Zhang, W. Klingsch, A. Schadschneider, and A. Seyfried, "Ordering in bidirectional pedestrian flows and its influence on the fundamental diagram," *J. Stat. Mech., Theory Exp.*, vol. 2012, no. 2, p. P02002, 2012.

[6] W. Guo, X. Wang, and X. Zheng, "Lane formation in pedestrian counterflows driven by a potential field considering following and avoidance behaviours," *Phys. A, Stat. Mech. Appl.*, vol. 432, pp. 87–101, Aug. 2015.

[7] J. Lee, T. Kim, J.-H. Chung, and J. Kim, "Modeling lane formation in pedestrian counter flow and its effect on capacity," *KSCE J. Civil Eng.*, vol. 20, no. 3, pp. 1099–1108, 2016.

[8] D. R. Parisi and C. O. Dorso, "Morphological and dynamical aspects of the room evacuation process," *Phys. A, Stat. Mech. Appl.*, vol. 385, no. 1, pp. 343–355, 2007.

[9] J. Tanimoto, A. Hagishima, and Y. Tanaka, "Study of bottleneck effect at an emergency evacuation exit using cellular automata model, mean field approximation analysis, and game theory," *Phys. A, Stat. Mech. Appl.*, vol. 389, no. 24, pp. 5611–5618, 2010.

[10] J. Dai, X. Li, and L. Liu, "Simulation of pedestrian counter flow through bottlenecks by using an agent-based model," *Phys. A, Stat. Mech. Appl.*, vol. 392, no. 9, pp. 2202–2211, 2013.

[11] X.-X. Yang, H.-R. Dong, X.-M. Yao, and X.-B. Sun, "Bottleneck effects on the bidirectional crowd dynamics," *Chin. Phys. B*, vol. 25, no. 12, p. 128901, 2016.

[12] R.-Y. Guo, "Simulation of spatial and temporal separation of pedestrian counter flow through a bottleneck," *Phys. A, Stat. Mech. Appl.*, vol. 415, pp. 428–439, Dec. 2014.

[13] N. Pelechano and N. I. Badler, "Modeling crowd and trained leader behavior during building evacuation," *IEEE Comput. Graph. Appl.*, vol. 26, no. 6, pp. 80–86, Nov./Dec. 2006.

[14] Z.-M. Fang, W.-G. Song, J. Zhang, and H. Wu, "A multi-grid model for evacuation coupling with the effects of fire products," *Fire Technol.*, vol. 48, no. 1, pp. 91–104, 2012.

[15] S. Cao, W. Song, W. Lv, and Z. Fang, "A multi-grid model for pedestrian evacuation in a room without visibility," *Phys. A, Stat. Mech. Appl.*, vol. 436, pp. 45–61, Oct. 2015.

[16] Y. Tajima and T. Nagatani, "Clogging transition of pedestrian flow in T-shaped channel," *Phys. A, Stat. Mech. Appl.*, vol. 303, nos. 1–2, pp. 239–250, 2002.

[17] J. Zhang, W. Klingsch, A. Schadschneider, and A. Seyfried, "Transitions in pedestrian fundamental diagrams of straight corridors and T-junctions," *J. Stat. Mech., Theory Exp.*, vol. 2011, no. 6, p. P06004, 2011.

[18] M. Craesmeyer and A. Schadschneider, "Simulation of merging pedestrian streams at T-junctions," *Transp. Res. Procedia*, vol. 2, no. 11, pp. 406–411, 2014.

[19] X. Shi, Z. Ye, N. Shiwakoti, D. Tang, C. Wang, and W. Wang, "Empirical investigation on safety constraints of merging pedestrian crowd through macroscopic and microscopic analysis," *Accident Anal. Prevention*, vol. 95, pp. 405–416, Oct. 2015.

[20] N. Shiwakoti, Y. Gong, X. Shi, and Z. Ye, "Examining influence of merging architectural features on pedestrian crowd movement," *Saf. Sci.*, vol. 75, pp. 15–22, Jun. 2015.

[21] Z. Fu, L. Yang, P. Rao, and T. Zhang, "Interactions of pedestrians interlaced in T-shaped structure using a modified multi-field cellular automaton," *Int. J. Mod. Phys. C*, vol. 24, no. 4, p. 1350024, 2013.

[22] H.-F. Jia, Y.-X. Li, L.-L. Yang, and Y.-N. Zhou, "Modeling the separating pedestrian flow in T-shaped passage based on guide sign," *Discrete Dyn. Nature Soc.*, vol. 2016, Jul. 2016, Art. no. 5625286.

[23] D. Helbing, M. Isobe, T. Nagatani, and K. Takimoto, "Lattice gas simulation of experimentally studied evacuation dynamics," *Phys. Rev. E, Stat. Phys. Plasmas Fluids Relat. Interdiscip. Top.*, vol. 67, no. 6, p. 067101, 2003.

[24] R. Y. Guo and H. J. Huang, "A mobile lattice gas model for simulating pedestrian evacuation," *Phys. A, Stat. Mech. Appl.*, vol. 387, nos. 2–3, pp. 580–586, 2008.

[25] H. Kuang, X. Li, T. Song, and S. Dai, "Analysis of pedestrian dynamics in counter flow via an extended lattice gas model," *Phys. Rev. E, Stat. Phys. Plasmas Fluids Relat. Interdiscip. Top.*, vol. 78, no. 6, p. 066117, 2008.

[26] V. J. Blue and J. L. Adler, "Cellular automata microsimulation for modeling bi-directional pedestrian walkways," *Transp. Res. B, Methodol.*, vol. 35, no. 3, pp. 293–312, 2001.

[27] T. Nagatani, "Freezing transition in bi-directional CA model for facing pedestrian traffic," *Phys. Lett. A*, vol. 373, no. 33, pp. 2917–2921, 2009.

[28] Q. Zhang, "Simulation model of bi-directional pedestrian considering potential effect ahead and behind," *Phys. A, Stat. Mech. Appl.*, vol. 419, pp. 335–348, Feb. 2015.

[29] D. Helbing, "Traffic and related self-driven many-particle systems," *Rev. Mod. Phys.*, vol. 73, no. 4, p. 1067, 2001.

[30] T. I. Lakoba, D. J. Kaup, and N. M. Finkelstein, "Modifications of the Helbing–Molnár–Farkas–Vicsek social force model for pedestrian evolution," *Simulation*, vol. 81, no. 5, pp. 339–352, 2005.

[31] R. Löhner, "On the modeling of pedestrian motion," *Appl. Math. Model.*, vol. 34, no. 2, pp. 366–382, 2010.

[32] J. van den Berg, M. Lin, and D. Manocha, "Reciprocal velocity obstacles for real-time multi-agent navigation," in *Proc. IEEE Int. Conf. Robot. Autom. (ICRA)*, May 2008, pp. 1928–1935.

[33] J. Van Den Berg *et al.*, "Reciprocal n-body collision avoidance," in *Robotics Research*. Berlin, Germany: Springer, 2011, pp. 3–19.

[34] S. Curtis and D. Manocha, "Pedestrian simulation using geometric reasoning in velocity space," in *Pedestrian and Evacuation Dynamics*. Zürich, Switzerland: Springer, 2014, pp. 875–890.

[35] K. Nagel and M. Schreckenberg, "A cellular automaton model for freeway traffic," *J. Phys. I France*, vol. 2, no. 12, pp. 2221–2229, Dec. 1992.

[36] S. Krauß, P. Wagner, and C. Gawron, "Metastable states in a microscopic model of traffic flow," *Phys. Rev. E, Stat. Phys. Plasmas Fluids Relat. Interdiscip. Top.*, vol. 55, no. 5, p. 5597, 1997.

[37] J. K. K. Yuen and E. W. M. Lee, "The effect of overtaking behavior on unidirectional pedestrian flow," *Saf. Sci.*, vol. 50, no. 8, pp. 1704–1714, 2012.

[38] R.-Y. Guo, S. C. Wong, H.-J. Huang, P. Zhang, and W. H. K. Lam, "A microscopic pedestrian-simulation model and its application to intersecting flows," *Phys. A, Stat. Mech. Appl.*, vol. 389, no. 3, pp. 515–526, 2010.

[39] M. Asano, T. Iryo, and M. Kuwahara, "Microscopic pedestrian simulation model combined with a tactical model for route choice behaviour," *Transp. Res. C, Emerg. Technol.*, vol. 18, no. 6, pp. 842–855, 2010.
[40] W. Zeng, P. Chen, H. Nakamura, and M. Iryo-Asano, "Application of social force model to pedestrian behavior analysis at signalized crosswalk," *Transp. Res. C, Emerg. Technol.*, vol. 40, pp. 143–159, Mar. 2014.
[41] D. Helbing and P. Molnár, "Social force model for pedestrian dynamics," *Phys. Rev. E, Stat. Phys. Plasmas Fluids Relat. Interdiscip. Top.*, vol. 51, no. 5, p. 4282, 1995.
[42] D. Helbing, I. Farkas, and T. Vicsek, "Simulating dynamical features of escape panic," *Nature*, vol. 407, no. 6803, pp. 487–490, 2000.
[43] Z. Yuan, H. Jia, M. Liao, L. Zhang, Y. Feng, and G. Tian, "Simulation model of self-organizing pedestrian movement considering following behavior," *Frontiers Inf. Technol. Electron. Eng.*, vol. 18, no. 8, pp. 1142–1150, 2017.
[44] Z. Yuan, H. Jia, L. Zhang, and L. Bian, "Simulation of pedestrian behavior in the collision-avoidance process considering their moving preferences," *Discrete Dyn. Nature Soc.*, vol. 2017, May 2017, Art. no. 3678268.
[45] L. Luo *et al.*, "Agent-based human behavior modeling for crowd simulation," *Comput. Animation Virtual Worlds*, vol. 19, nos. 3–4, pp. 271–281, 2008.
[46] A. Best, S. Narang, S. Curtis, and D. Manocha, "DenseSense: Interactive crowd simulation using density-dependent filters," in *Proc. ACM SIGGRAPH/Eurographics Symp. Comput. Animation*, 2014, pp. 97–102.
[47] L. Luo, C. Chai, S. Zhou, and J. Ma, "Modeling gap seeking behaviors for agent-based crowd simulation," in *Proc. 29th Int. Conf. Comput. Animation Social Agents*, 2016, pp. 37–43.
[48] L. Luo, C. Chai, J. Ma, S. Zhou, and W. Cai, "ProactiveCrowd: Modelling proactive steering behaviours for agent-based crowd simulation," *Comput. Graph. Forum*, vol. 37, no. 1, pp. 375–388, 2018.
[49] S. Narang, A. Best, S. Curtis, and D. Manocha, "Generating pedestrian trajectories consistent with the fundamental diagram based on physiological and psychological factors," *PLoS ONE*, vol. 10, no. 4, p. e0117856, 2015.
[50] M. Vlachos, G. Kollios, and D. Gunopulos, "Discovering similar multidimensional trajectories," in *Proc. IEEE 18th Int. Conf. Data Eng.*, Feb./Mar. 2002, pp. 673–684.
[51] Z. Zhang, K. Huang, and T. Tan, "Comparison of similarity measures for trajectory clustering in outdoor surveillance scenes," in *Proc. IEEE 18th Int. Conf. Pattern Recognit. (ICPR)*, vol. 3, Aug. 2006, pp. 1135–1138.

ZHILU YUAN was born in Heilongjiang, China. He received the Ph.D. degree from the School of Transportation, Jilin University, in 2017. He currently holds a postdoctoral position with the School of Architecture and Urban Planning, Research Institute for Smart Cities, Shenzhen University, Shenzhen, China. His research interests is transportation planning, including traffic flow modeling, pedestrian flow modeling, pedestrian simulation research, related software, and theories and applications of transportation planning.

RENZHONG GUO was born in Jiangsu, China. He received the Ph.D. degree in geography from Franche-Comté University, France, in 1990. He is an Academician of the Chinese Academy of Engineering, a Professor and Doctoral Supervisor with Shenzhen University, and a Geographical Information Engineering Expert. He has been involved in research and development of Cartography, GIS, and construction strategy of digital city for a long time. Great achievements are also being made in theories and methods of geographical information system, and information engineering of land resource management.

SHENGJUN TANG was born in Jiangxi, China, in 1991. He received the Ph.D. degree in cartography from the Wuhan University of China, in 2017. He joined the Shenzhen University, in 2017, where he currently holds a postdoctoral position with the School of Architecture and Urban Planning, Research Institute for Smart Cities. His main research interests are 3D SLAM, 3D GIS, and indoor modeling 3D.

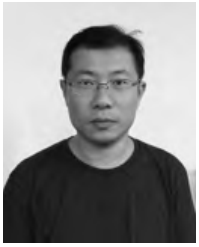

BIAO HE was born in Wuhan, China, in 1983. He received the Ph.D. degree from the Wuhan University of China, in 2011. He is currently an Associate Professor with the School of Architecture and Urban Planning, Research Institute for Smart Cities, Shenzhen University, Shenzhen, China. He is mainly involved in research on 3D GIS and VGE, and city big data management.

LEI BIAN was born in Heilongjiang, China, in 1986. He received the Ph.D. degree in fluid mechanics and applied mathematics from Peking University, Beijing, China, in 2016.

He was a Research Assistant with the Beijing Computational Science Research Center, Beijing, China, in 2016. From 2016 to 2018, he held a postdoctoral position with the Labratoire de Mathématiques Raphaël Salem, C.N.R.S, University of Rouen, France, and the University of Wisconsin at Madison, respectively. He joined the School of Architecture and Urban Planning, Research Institute for Smart Cities, Shenzhen University, Shenzhen, China, as an Assistant Professor, at the end of 2018.

His research interests include numerical analysis, quantum fluid mechanics, PDE, CAVH, and artificial intelligence.

YOU LI received the Ph.D. degree in geographic information science from the Wuhan University of China, in 2017. He is currently holding a postdoctoral position with the School of Architecture and Urban Planning, Research Institute for Smart Cities, Shenzhen University. His main interests include LiDAR processing and object recognition from LiDAR data.